

Probing the collective excitations of a spinor polariton fluid

M. Van Regemortel,^{1,*} M. Wouters,¹ and F. M. Marchetti²

¹*TQC, Universiteit Antwerpen, Universiteitsplein 1, B-2610 Antwerpen, Belgium*

²*Departamento de Física Teórica de la Materia Condensada & Condensed Matter Physics Center (IFIMAC), Universidad Autónoma de Madrid, Madrid 28049, Spain*

(Dated: May 23, 2022)

We propose a pump-probe set-up to analyse the properties of the collective excitation spectrum of a spinor polariton fluid. By using a linear response approximation scheme, we carry on a complete classification of all excitation spectra, as well as their intrinsic degree of polarisation, in terms of two experimentally tunable parameters only, the mean-field polarisation angle and a rescaled pump detuning. We evaluate the system response to the external probe, and show that the transmitted light can undergo a spin rotation along the dispersion for spectra that we classify as diffusive-like. We show that in this case, the spin flip predicted along the dispersion is enhanced when the system is close to a parametrically amplified instability.

PACS numbers: 71.36.+c, 03.75.Mn, 03.75.Kk

I. INTRODUCTION

Strongly coupled matter-light systems, such as exciton-polariton microcavities, have recently witnessed an escalating interest thanks to the simultaneous versatility in manipulating and probing their intrinsic properties. Resulting from the strong coupling of cavity photons and quantum well excitons, exciton-polaritons display unique properties deriving from both their constituents — for recent reviews see Refs.¹⁻⁴. In particular, the resonant excitation scheme, where polaritons are directly injected by an external laser near the energy of the lower polariton dispersion, allows to experimentally access a unique accurate tuning of the system parameters, such as the polariton density, current properties, as well as their phase, which is locked to the one of the external pump.

Much work has been already done both theoretically as well as experimentally for resonantly pumped single component polariton fluids in the pump-only configuration⁵⁻¹¹, i.e., where only the pump state is occupied and no parametric scattering occurs. Particular interest was dedicated in analysing the properties of the collective spectrum of excitations and relate them to the system superfluid behaviour⁵⁻⁷. Here, the spectrum could be classified either as gapped, or linear, or else diffusive-like, in terms of a single parameter, the renormalised pump detuning. Interestingly, diffusive-like spectra in non-equilibrium fluids have been shown to be related to parametric scattering and amplification⁶ and to the occurrence of a negative drag force of the single component polariton fluid when scattering against a localised defect¹².

In this article we consider the case of a spinor, i.e., two-component, polariton fluid, by explicitly including the polarisation degrees of freedom. It has been observed that, for fixed pump detuning and degree of polarisation, the system undergoes a spin flip and a subsequent hysteresis curve when varying the pump power, promoting this system as an ideal environment where to realise an optical spin switch¹³⁻¹⁵ or a logical gate¹⁶. Interestingly,

it has been recently demonstrated that spinor polariton systems have tunable cross-spin interaction properties¹⁷.

In previous recent work¹⁸, the spectrum of elementary excitation for a resonantly excited pump-only polariton fluid including the spin degrees of freedom was analysed. In that work, by considering for simplicity only the limiting cases of a purely linearly polarised fluid and a purely circularly polarised one, the focus was on the superfluid properties of the system and the possibility of reproducing a linear spectrum when the pump detuning compensates exactly the interaction-induced blueshift.

Here, we propose a pump-probe set-up tailored for analysing the properties of the collective excitation spectrum. We show that in the linear response approximation scheme, valid for a weak probe beam, the spectrum of excitations can be evaluated analytically even in the generic case of an elliptically polarised spinor polariton fluid. Further, for fixed interaction strengths, the spectrum can be completely classified in terms of only two experimentally tunable parameters: the mean-field polarisation angle and a rescaled pump detuning. Now the number of different class sets of spectra is much larger compared with the single fluid case. Yet, depending how the two opposite circular polarisation degrees of freedom mix together in the spectra, we can single out three larger sets where the behaviour of the spectrum intrinsic degree of polarisation is qualitatively different. We name them as *gapped*, *0-diffusive*, and *ω -diffusive*; these regions in the two-parameter space are separated by conditions for which the spectrum can be *linear*. While for gapped spectra, there is no mixing of opposite circular polarisation degrees of freedom, for both diffusive-like spectra, the mixing is responsible for flips of the intrinsic spin degree of polarisation along the branches. Further, we evaluate the system response to the external probe and analyse the properties of the transmitted light and its relations to the collective excitation spectrum. In particular we determine the properties of the spin flip along the branches for diffusive-like spectra and how the spin rotation is larger, the closer the system is to a parametric

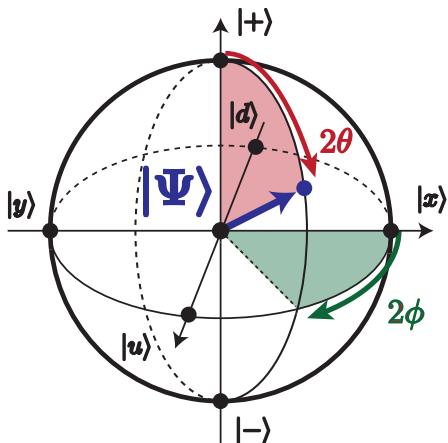


FIG. 1. (Color online) Representation of the Poincaré sphere illustrating all possible light polarisations. The basis of left and right circular polarisation (perpendicular to the microcavity plane), $\{|+\rangle, |-\rangle\}$, are the sphere north and south poles, respectively. In contrast, all linear polarisation states (parallel to the cavity mirror) lie on the equator and for those one can choose two alternative basis, either $\{|x\rangle, |y\rangle\}$ or $\{|u\rangle, |d\rangle\}$. A generic elliptically polarised state $|\Psi\rangle$ lies everywhere on the sphere, except at the poles and at the equator, and is defined by a polar angle 2θ (characterising the degree of mixing between circular and linear polarisation) and an azimuthal angle 2ϕ (characterising the in-plane polarisation orientation with respect to an x -linearly-polarised state).

instability.

The paper is organised as follows: In Sec. II, we present the generalised Gross-Pitaevskii equation that describes the resonantly pumped spinor fluid and briefly discuss its mean-field solutions from existing literature. We introduce the proposed pump-probe scheme in Sec. III and discuss the linear response approximation scheme. The spectrum of collective excitations is evaluated in Sec. III A, where we derive a “phase diagram” classifying all possible spectral categories. In Sec. III B we derive the emission properties of the intrinsic degree of polarization for each spectrum branch. Finally, in Sec. III C, we evaluate the spinor polariton fluid response to the additional probe beam and relate its properties to the spectrum intrinsic properties previously discussed.

II. MODEL

The dynamics of resonantly pumped polaritons is described by a Gross-Pitaevskii equation (GPE) for the polariton field generalised to include the effects of the polariton finite lifetime $2\pi\hbar/\gamma$, as well as the ones of an external laser that resonantly injects polaritons into the microcavity⁴. Here, we consider a simplified model which involves the lower polariton (LP) branch only. The resonant pumping scheme we will consider implies populating a specific LP state with low momentum, allowing us

to neglect the occupation of the upper polariton branch. Further, we include the two degrees of freedom of the polariton polarisation in the left $|+\rangle$ and right $|-\rangle$ circular polarisation basis^{1,19} — see Fig. 1 for a schematic representation of the Poincaré sphere for light polarisation. The generalised GPE equation for the spinor LP field $\Psi_{\pm}(\mathbf{r}, t)$ reads as ($\hbar = 1$ throughout):

$$i\partial_t\Psi_{\pm} = \left[\omega_{LP}(-i\nabla) - i\frac{\gamma}{2} + \alpha_1|\Psi_{\pm}|^2 + \alpha_2|\Psi_{\mp}|^2 \right] \Psi_{\pm} + \mathcal{F}_{\pm}(\mathbf{r}, t). \quad (1)$$

Here, the homogeneous pump term $\mathcal{F}_{\pm}(\mathbf{r}, t)$,

$$\mathcal{F}_{\pm}(\mathbf{r}, t) = f_{\pm}^p e^{i(\mathbf{k}_p \cdot \mathbf{r} - \omega_p t)}, \quad (2)$$

resonantly injects polaritons with a momentum \mathbf{k}_p and an energy ω_p close to the bottom of the LP dispersion $\omega_{LP}(\mathbf{k})$. For this reason, we consider a quadratic approximate of such a dispersion, $\omega_{LP}(\mathbf{k}) \simeq_{\mathbf{k} \rightarrow 0} \frac{\hbar^2 k^2}{2m}$, where m is the LP mass and we have fixed $\omega_{LP}(0) = 0$. In (1) we can thus substitute $\omega_{LP}(-i\nabla) \simeq -\frac{\nabla^2}{2m}$.

Polariton interaction properties depend on their polarisation component. With α_1 we denote the interaction strength between polaritons in the same circular polarisation state; this is repulsive, $\alpha_1 > 0$, like the interaction strength between excitons with the same spin²⁰; when excitons mix with photons to form polaritons, one can show that the resulting strength α_1 weakly depends on the LP properties such as the photon-exciton detuning and the Rabi splitting²¹. Instead α_2 is the interaction strength between polaritons with opposite circular polarisations. Interestingly, it has been very recently shown that this inter-polarisation coupling can be tuned by means of a bipolariton Feshbach resonance mechanism¹⁷ from being attractive to repulsive, by simply changing the value of the LP photon-exciton detuning. Here, we assume to be far from such a resonance, in a regime where α_2 is weakly attractive, and in particular we fix $\alpha_2/\alpha_1 = -0.1$ ²¹. Note that, for an equilibrium homogeneous spinor Bose-Einstein condensate at zero temperature (i.e., described by the same GPE with no pumping nor decaying term and chemical potentials fixing the particle number in each condensate), attraction between opposite components implies a collapse of the system, i.e., mechanical instability, unless $|\alpha_2|/\alpha_1 < 1$ ²². In this regime, the results obtained here for the polariton spinor fluid resonantly pumped by an external laser do not qualitatively depend on the particular value chosen for the ratio $|\alpha_2|/\alpha_1$. Interestingly, the anisotropy of polariton-polariton interactions, characterised by the ratio α_2/α_1 , was shown to be responsible for the existence of effective magnetic monopoles in the form of half-integer topological defects²³ and screening of a magnetic field, the *spin Meissner effect*²⁴.

For a homogeneous pump-only scheme as in Eq. (2), the GPE dynamics (1) is solved by the following mean-field plane-wave steady-state solution,

$$\Psi_{\pm}(\mathbf{r}, t) = \psi_{\pm} e^{i(\mathbf{k}_p \cdot \mathbf{r} - \omega_p t)}, \quad (3)$$

i.e., by assuming that the pump only populates the LP state with the very same momentum \mathbf{k}_p and energy ω_p . Note that in this resonant pumping scheme, the polariton fluid phase is locked to the one of the external laser. One can then find how the intensity of the emission in the two polarisation states, $|\psi_{\pm}|^2$, vary when changing the system parameters, e.g., by increasing the pump strength and its degree of polarisation, via the parameters f_{\pm} . Much work has been recently carried out to investigate the mean-field properties of spinor polariton fluids, including the possibility for multistable behaviour — see, e.g., Refs.^{14,25}. In particular, for a single-component resonantly pumped polariton fluid, multistability appears when the polariton population goes through an hysteresis loop as a function of the pump intensity: When resonantly pumping above the LP dispersion, an increase of the pump power implies an interaction induced blue-shift of the LP energy towards resonance and thus a sudden increase of the LP population. When instead the pump power is lowered, a sudden drop occurs at lower pump powers, resulting in a region on multistability. For spinor fluids, it has been found that the most-populated spin component is subject to an hysteresis loop, while the less-populated component undergoes a smooth intensity increase^{13,14,25}. Interestingly, this mechanism has been proposed for realising an optical spin switch¹⁵.

We refer the reader to the literature for the mean-field analysis, and instead assume here that the system is pumped in such a way as to induce a given degree of polarisation for the mean-field solution. This is completely characterised, as any general elliptical polarisation state, by both a polar angle θ_0 and an azimuthal angle ϕ_0 (see Fig. 1), respectively defined as:

$$\cos(2\theta_0) = \frac{|\psi_+|^2 - |\psi_-|^2}{|\psi_+|^2 + |\psi_-|^2} \quad (4)$$

$$\tan(2\phi_0) = \frac{\Im(\psi_+^* \psi_-)}{\Re(\psi_+^* \psi_-)}. \quad (5)$$

Without loss of generality, we can however assume that the pump induces a mean-field state with $\phi_0 = 0$, as this simply corresponds to a choice of the reference coordinate system and any other elliptically polarised state can be obtained by rotating the microcavity plane. We then study how the collective excitation spectrum for such spinor polariton fluid, as well as its response to a weak-probe beam, change when varying $\theta_0 \in [0, \pi/4]$ — the other interval $\theta_0 \in [\pi/4, \pi/2]$ is symmetric for $\psi_+ \leftrightarrow \psi_-$.

III. LINEAR RESPONSE TO A WEAK PROBE BEAM

In order to probe the spectrum of collective excitations of a resonantly pumped spinor polariton fluid, we introduce an additional weak beam which can be shined at several energies and angles, different from the pump ones. In particular, referring to the schematic setup for

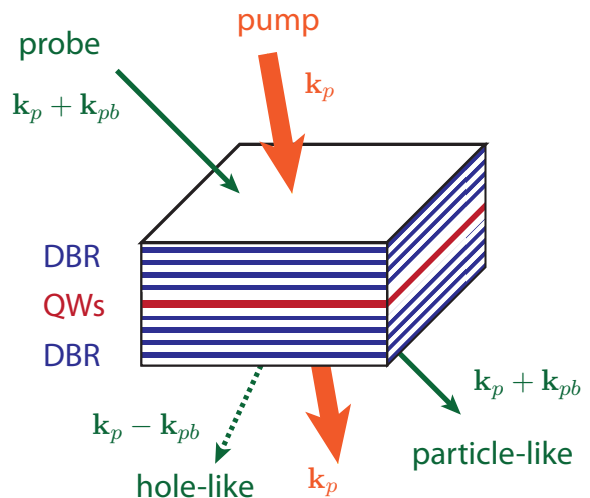


FIG. 2. (Color online) Schematic setup for the pump-probe experiments designed to measure the collective excitation spectrum of a spinor polariton fluid. The cavity (composed of two distributed Bragg mirrors [DBR] with embedded quantum wells [QWs]) is resonantly excited with a pump, with a momentum \mathbf{k}_p and an energy ω_p close to the LP dispersion. A second weak probe beam, with momentum $\mathbf{k}_p + \mathbf{k}_{pb}$, and energy $\omega_p + \omega_{pb}$ that can be scanned at different values, is used to probe the system collective excitation spectrum. The transmitted light will have a “particle-like” component emitting at the direction corresponding to $\mathbf{k}_p + \mathbf{k}_{pb}$ and a “hole-like” component at $\mathbf{k}_p - \mathbf{k}_{pb}$.

the proposed pump-probe experiment in Fig. 2, we consider a homogeneous pump term as in (2) and add to it a homogeneous probe beam with strength f_{\pm}^{pb} , shined at a direction $\mathbf{k}_p + \mathbf{k}_{pb}$ (with $\mathbf{k}_{pb} \neq 0$) and an energy $\omega_p + \omega_{pb}$:

$$\mathcal{F}_{\pm}(\mathbf{r}, t) = e^{i(\mathbf{k}_p \cdot \mathbf{r} - \omega_p t)} \left[f_{\pm}^p + f_{\pm}^{pb} e^{i(\mathbf{k}_{pb} \cdot \mathbf{r} - \omega_{pb} t)} \right]. \quad (6)$$

The wave-vector \mathbf{k}_{pb} should not be confused with the probe direction, rather it corresponds to the probe momentum relative to the pump momentum \mathbf{k}_p .

We assume that the system is only weakly perturbed by the probe; therefore, we can apply a linear-response approximation, where only two other states are weakly populated aside the mean-field state (3)²⁶:

$$\Psi_{\pm}(\mathbf{r}, t) = e^{i(\mathbf{k}_p \cdot \mathbf{r} - \omega_p t)} \left[\psi_{\pm} + u_{\pm} e^{i(\mathbf{k}_{pb} \cdot \mathbf{r} - \omega_{pb} t)} + v_{\pm}^* e^{-i(\mathbf{k}_{pb} \cdot \mathbf{r} - \omega_{pb} t)} \right]. \quad (7)$$

Note that, although the polariton sample is only excited at two directions, the pump \mathbf{k}_p and the probe one $\mathbf{k}_p + \mathbf{k}_{pb}$, transmission must also include an additional signal at $\mathbf{k}_p - \mathbf{k}_{pb}$. This is a consequence of polariton interactions which mix the particle-like excitations u_{\pm} , resulting from adding a particle into the mean-field state, with the hole-like degrees of freedom v_{\pm} , which are excited by instead removing a particle. Thus, as schematically

drawn in Fig. 2, we expect the weak probe to imply a transmission in both directions $\mathbf{k}_p \pm \mathbf{k}_{pb}$. We will analyse in Sec. III C the properties of both transmission signals, as well as the relation to the intrinsic properties of the collective excitation spectrum.

The system response to the probe is easily evaluated by substituting (7) into the GPE equation (1) and by expanding at first order in both the probing field strength f_{\pm}^{pb} and the fluctuation terms above mean-field, u_{\pm} and v_{\pm} .

We obtain four coupled equations diagonal in momentum space

$$\left(\omega_{pb}\hat{\mathbb{I}} - \hat{\mathcal{L}}_{\mathbf{k}_{pb}}\right) \mathbf{w} = \mathbf{f}^{pb}, \quad (8)$$

where response and probe have been rearranged into four component vectors, $\mathbf{w} = (u_+, v_+, u_-, v_-)^T$ and $\mathbf{f}^{pb} = (f_+^{pb}, 0, f_-^{pb}, 0)^T$. The Bogoliubov operator $\hat{\mathcal{L}}_{\mathbf{k}}$ can be written in terms of its polarisation components,

$$\hat{\mathcal{L}}_{\mathbf{k}} = \begin{pmatrix} \hat{\mathcal{M}}_{++,\mathbf{k}} & \hat{\mathcal{M}}_{+-,\mathbf{k}} \\ \hat{\mathcal{M}}_{-+,\mathbf{k}} & \hat{\mathcal{M}}_{--,\mathbf{k}} \end{pmatrix}, \quad (9)$$

which are given by the expressions ($i = +, -$):

$$\hat{\mathcal{M}}_{ii,\mathbf{k}} = \begin{pmatrix} \tilde{\epsilon}_{i,\mathbf{k}} + \mathbf{k} \cdot \mathbf{v}_p - i\frac{\gamma}{2} & \alpha_1 \psi_i^2 \\ -\alpha_1 \psi_i^{*2} & -\tilde{\epsilon}_{i,\mathbf{k}} + \mathbf{k} \cdot \mathbf{v}_p - i\frac{\gamma}{2} \end{pmatrix} \quad (10)$$

$$\hat{\mathcal{M}}_{+-,\mathbf{k}} = \alpha_2 \begin{pmatrix} \psi_+^* \psi_- & \psi_+ \psi_- \\ -\psi_+^* \psi_-^* & -\psi_+ \psi_-^* \end{pmatrix}. \quad (11)$$

The parameters appearing in the diagonal components of the Bogoliubov operator are the fluid velocity $\mathbf{v}_p = \mathbf{k}_p/m$ and the following energy term:

$$\tilde{\epsilon}_{\pm,\mathbf{k}} = \epsilon_{\pm,\mathbf{k}} + \alpha_1 |\psi_{\pm}|^2 \quad (12)$$

$$\epsilon_{\pm,\mathbf{k}} = \frac{\mathbf{k}^2}{2m} - \Delta_{\pm} \quad (13)$$

$$\Delta_{\pm} = \omega_p - \left(\frac{\mathbf{k}_p^2}{2m} + \alpha_1 |\psi_{\pm}|^2 + \alpha_2 |\psi_{\mp}|^2 \right). \quad (14)$$

In particular, Δ_{\pm} can be interpreted as the effective pump detuning, i.e., the energy difference between the laser frequency ω_p and the LP dispersion at momentum \mathbf{k}_p renormalised by the interaction induced blue-shift due to both the intra-polarisation coupling $\alpha_1 |\psi_{\pm}|^2$ and the inter-polarisation one $\alpha_2 |\psi_{\mp}|^2$.

Before analysing the properties of the probe response \mathbf{w} starting from Eq. (8) (Sec. III C), we discuss first the collective excitation spectrum of the spinor polariton fluid and its intrinsic properties (Sec. III A), including its degree of polarisation (Sec. III B).

A. Excitation spectrum of the spinor polariton fluid

For a general wave-vector \mathbf{k} (as for \mathbf{k}_{pb} , here \mathbf{k} is assumed to be measured with respect to the pump wave-

vector \mathbf{k}_p), the different branches of the spectrum of excitations are the eigenvalues of the Bogoliubov operator $\hat{\mathcal{L}}_{\mathbf{k}}$ and thus are evaluated starting from the equation:

$$\det \left(\hat{\mathcal{L}}_{\mathbf{k}} - \omega \hat{\mathbb{I}} \right) = 0, \quad (15)$$

or equivalently finding the roots of the following polynomial equation:

$$\prod_{i=+,-} \left[\left(\omega + i\frac{\gamma}{2} - \mathbf{k} \cdot \mathbf{v}_p \right)^2 - E_{i,\mathbf{k}}^2 \right] = -4\alpha_2^2 \prod_{i=+,-} (\epsilon_{i,\mathbf{k}} |\psi_i|^2).$$

This can be solved exactly, resulting in four branches of the spectrum, which, as explained later, we label with a new index $a = u_{\uparrow}, v_{\uparrow}, u_{\downarrow}, v_{\downarrow}$:

$$\omega_{\mathbf{k}}^{(a)} = \mathbf{k} \cdot \mathbf{v}_p - i\frac{\gamma}{2} + \eta_{u,v} \left[\frac{E_{+,\mathbf{k}}^2 + E_{-,\mathbf{k}}^2}{2} + \sigma_{\uparrow,\downarrow} \sqrt{\left(\frac{E_{+,\mathbf{k}}^2 - E_{-,\mathbf{k}}^2}{2} \right)^2 + 4\alpha_2^2 \prod_{i=+,-} (\epsilon_{i,\mathbf{k}} |\psi_i|^2)} \right]^{1/2} \quad (16)$$

where $\eta_{u,v} = \pm 1$ for the particle-like and hole-like components respectively and $\sigma_{\uparrow,\downarrow} = \pm 1$. Here, the energy

$$E_{\pm,\mathbf{k}} = \sqrt{\epsilon_{\pm,\mathbf{k}} (\epsilon_{\pm,\mathbf{k}} + 2\alpha_1 |\psi_{\pm}|^2)}, \quad (17)$$

determines the excitation spectrum of two independent fluids with opposite circular polarisations, which is given by^{5,27}

$$\lim_{\alpha_2 \rightarrow 0} \omega_{\mathbf{k}}^{(a)} = \mathbf{k} \cdot \mathbf{v}_p - i\frac{\gamma}{2} + \eta_{u,v} E_{\pm,\mathbf{k}}. \quad (18)$$

When setting $\psi_- = 0$ (circular polarization) or $\psi_+ = \psi_-$ (linear polarization), one recovers the limiting expressions derived in Ref.¹⁸.

Note that, because of interactions, polarisation and particle-hole degrees of freedom do in general mix together along the dispersion of each spectrum branch. Yet, the choice of the index $a = u_{\uparrow}, v_{\uparrow}, u_{\downarrow}, v_{\downarrow}$ for labeling the four branches of the excitation spectrum is motivated by the fact that, at large momenta there is no mixing between the particle-like ($u_{\uparrow,\downarrow}$) and hole-like ($v_{\uparrow,\downarrow}$) degrees of freedom, while the same does not hold of $+$ and $-$ polarisation states that do remain coupled — i.e., as we will see later, the intrinsic polarisation of these branches can never be purely circularly $+$ or $-$ polarised even at large momenta, where the energy becomes

$$\lim_{k \rightarrow \infty} \omega_{\mathbf{k}}^{(u_{\uparrow}, v_{\uparrow}, u_{\downarrow}, v_{\downarrow})} = \mathbf{k} \cdot \mathbf{v}_p - i\frac{\gamma}{2} + \eta_{u,v} \left[\frac{(\mathbf{k} + \eta_{u,v} \mathbf{k}_p)^2}{2m} + 2\alpha_1 |\psi_{\uparrow,\downarrow}|^2 + \alpha_2 |\psi_{\downarrow,\uparrow}|^2 \right], \quad (19)$$

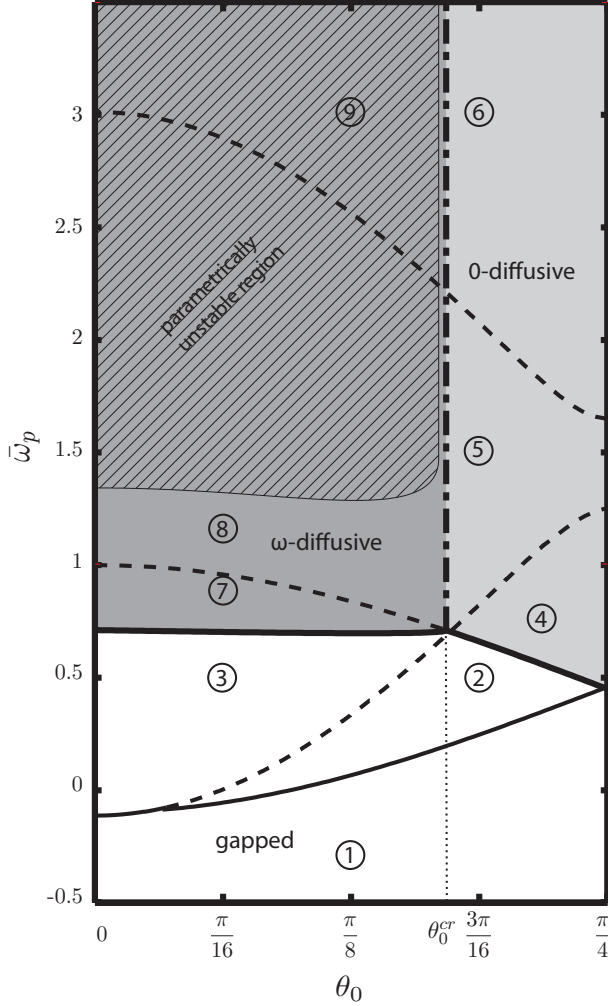


FIG. 3. “Phase diagram” showing the different classes of spectra of a spinor polariton fluid as a function of the two dimensionless parameters $\bar{\omega}_p$ (20) and the mean-field polarisation angle θ_0 (4) for $\alpha_2/\alpha_1 = -0.1$ —the case of left circular polarisation corresponds to $\theta_0 = 0$, while the one of linear polarisation to $\theta_0 = \pi/4$. The labels 1 – 9 correspond to the exact parameter values chosen for the corresponding spectra plotted in Fig. 4. The value of the critical polarisation angle θ_0^{cr} (21) is marked with a dash-dotted line. The white region (*gapped*) includes the spectra 1 – 3 characterised by a gap for the + branches; the clear-gray region (*0-diffusive*) are the spectra 4 – 6 displaying diffusive behaviour at zero energy, while the dark-gray region (*ω -diffusive*) are the spectra 7 – 9 where a diffusive region can also be at finite energy (see text). The striped region is the parametrically unstable region for $\gamma = 1.5\mathcal{E}$.

where $\psi_{\uparrow,\downarrow} \equiv \psi_{+,-}$. For this reason, we introduce a new notation \uparrow,\downarrow for the branch index $a = (u_{\uparrow}, v_{\uparrow}, u_{\downarrow}, v_{\downarrow})$, indicating that the pure circular polarisation degrees of freedom \pm are always coupled.

We now classify all possible different types of excitation spectra (see Fig. 4) and how these evolve from one type to the other by changing the system parameters, as represented in the “phase diagram” of Fig. 3.

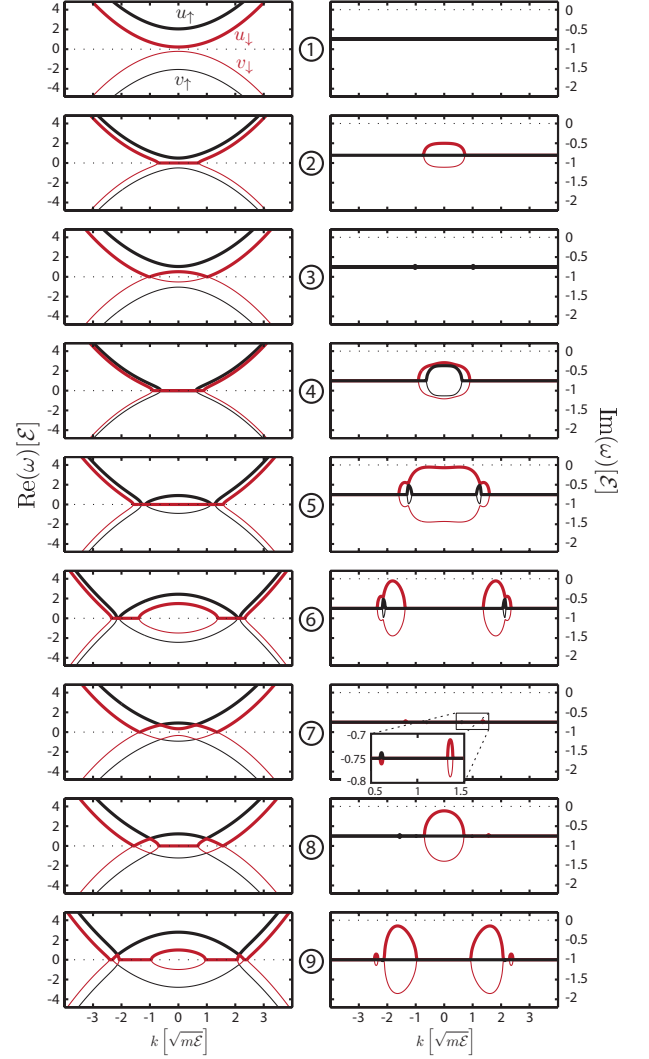


FIG. 4. (Color online) Different types of excitation spectra (real part $\Re\omega_{\mathbf{k}}^{(a)}$ in the left panels and imaginary part $\Im\omega_{\mathbf{k}}^{(a)}$ in the right panels) allowed for a spinor polariton fluid for $\alpha_2/\alpha_1 = -0.1$ and for a pump wave-vector $\mathbf{k}_p = 0$. The energy ω is measured in units of $\mathcal{E} = \alpha_1(|\psi_+|^2 + |\psi_-|^2)$, while momentum (plots are cuts at $k_y = 0$) in units of $\sqrt{m\mathcal{E}}$. Thick (thin) black lines are the u_{\uparrow} (v_{\uparrow}) branches, while thick (thin) red-gray lines are the u_{\downarrow} (v_{\downarrow}) branches. The labels 1 – 9 correspond to the very same parameters $(\bar{\omega}_p, \theta_0)$ shown in the “phase diagram” of Fig. 3, where the corresponding labels appear. The polariton decay rate is fixed to $\gamma = 1.5\mathcal{E}$ for the spectra 1 – 8 and to $\gamma = 2\mathcal{E}$ for spectrum 9.

Interestingly, for a fixed interaction strength ratio α_2/α_1 ($= -0.1$ in the figures), only two dimensionless independent parameters are sufficient in order to classify all possible different types of spectra of a resonantly pumped spinor polariton fluid: 1) the mean-field polarisation angle θ_0 (4) and 2) the dimensionless pump energy rescaled by the “self-

interaction" energy $\mathcal{E} = \alpha_1(|\psi_+|^2 + |\psi_-|^2)$:

$$\bar{\omega}_p = \frac{\omega_p}{\alpha_1(|\psi_+|^2 + |\psi_-|^2)}. \quad (20)$$

By means of these two parameters only we can fully classify all the allowed spectrum typologies. Note in fact that the value of the pump momentum \mathbf{k}_p has the sole effect of tilting the spectrum dispersion; in the quadratic approximation for the LP dispersion considered here, this corresponds to a Galilean transformation.²⁸ For this reason, we plot, without loss of generality, the spectra of Fig. 4 for a pump in the orthogonal direction to the cavity growth, $\mathbf{k}_p = 0$.

In the absence of inter-polarisation interaction, $\alpha_2 = 0$, and for equal spin populations, $|\psi_+| = |\psi_-|$, both sign and value of a single parameter, the rescaled interaction renormalised pump detuning $\bar{\Delta} = \Delta/\alpha_1|\psi_+|^2$, determine the four types of possible spectra^{5,27}: 1) for $\Delta < 0$ the spectrum is *gapped*; 2) the gap closes to zero for $\Delta = 0$ and the dispersion is *linear* at low momenta; while for $\Delta > 0$, particle and hole branches of the spectrum real part touch together in either 3) one ($\bar{\Delta} \leq 2$) or 4) two ($\bar{\Delta} > 2$) separate momentum intervals — note that Fig. 4 is a cut at $k_y = 0$, so intervals for those plots in reality corresponds to rings in the two-dimensional \mathbf{k} -space. Both cases 3) and 4) are generally named as *diffusive* spectra. Note that the linear spectrum is allowed for a single value of the detuning Δ , and thus even if the types of different spectra for $\alpha_2 = 0$ are four in total, the finite interval regions in Δ displaying different spectra are only three (and $\Delta = 0$ represents a separating point between two of these regions). For the spinor case, the minimal set of independent dimensionless parameters characterising the spectrum is instead formed by θ_0 and $\bar{\omega}_p$. Note that by rescaling the pump detuning Δ_{\pm} (14) by the self-interaction energy \mathcal{E} would still lead to a parameter depending on θ_0 .

For a coupled spinor fluid, with $\alpha_2 \neq 0$, the classes of different spectra increase from four to eighteen; by counting the parameter finite regions only (and excluding the separating lines), this corresponds to nine regions of different spectra compared to the three of the previous $\alpha_2 \rightarrow 0$ limit case. The proliferation of different types of spectra is due to the presence of two nested square roots in Eq. (16). Which of the four branches have a degenerate real part as well as in how many momentum intervals degeneracy occurs, depends on the sign of both square root arguments. All nine possibilities for the spectra are plotted in Fig. 4 and the various "phase diagram" regions in the $(\bar{\omega}_p, \theta_0)$ parameter space where such spectra are allowed are plotted in Fig. 3.

For both negative as well as small positive values of the renormalised dimensionless pump energy detuning, $\bar{\omega}_p$, the spectrum is fully *gapped*, i.e., none of the four branches mix together (panel 1 in Fig. 4). By increasing the value of $\bar{\omega}_p$ at fixed θ_0 , the \uparrow branches (black lines) are still gapped, while the real part of the particle-like u_{\downarrow} (thick red-gray) and hole-like v_{\downarrow} (thin red-gray) branches

undergo the same changes as previously described for a single component fluid: they touch each other first in a single momentum interval (panel 2) and then in two separate momentum intervals (panel 3).

Even if for panels 2 and 3 the \downarrow branches have a diffusive-like character, with an imaginary part deviating from the polariton lifetime, $\Im\omega \neq -\gamma/2$, in all the three regimes 1 – 3 described, the \uparrow and \downarrow real part branches are never degenerate and hence do not mix one with the other, so that each maintains its own character: we group the three cases as *gapped* spectra (white region of Fig. 3).

When we further increase the value of $\bar{\omega}_p$, the opposite polarisation branches can however mix together and the spectrum evolves differently depending on the value of the mean-field polar angle θ_0 : in particular it either changes from the type 3 to 7 if $\theta_0 < \theta_0^{\text{cr}}$, or from 2 to 4 if $\theta_0 > \theta_0^{\text{cr}}$, where the critical angle θ_0^{cr} is given by:

$$\cos(2\theta_0^{\text{cr}}) = \frac{1}{2} \sqrt{1 + \frac{\alpha_2}{\alpha_1}}. \quad (21)$$

For $\alpha_2/\alpha_1 = -0.1$, this critical value of the polarisation angle is given by $\theta_0^{\text{cr}} \simeq 0.54$. The dash-dotted line in Fig. 3 indicates where θ_0^{cr} determines the boundary between these two cases. The difference between the two is how the \uparrow and \downarrow branches mix together and at which energy the mixing happens. For $\theta_0 > \theta_0^{\text{cr}}$, there is only mixing of the branches at zero energy, as for the three spectra 4–6, which we group under the naming *0-diffusive* (clear gray region of Fig. 3). When $\theta_0 < \theta_0^{\text{cr}}$, the spectra are characterized by the presence of a diffusive momentum region at finite energy, as for the spectra 7–9, that we group under the naming ω -*diffusive* spectra (dark gray region of Fig. 3).

If we increase $\bar{\omega}_p$ for $\theta_0 > \theta_0^{\text{cr}}$, the branches transforms via different *0-diffusive* phases. For the spectrum of type 4 all four branches real parts are degenerate at $\omega = 0$ around $\mathbf{k} = 0$, this then evolves to a zero energy degeneracy in different parts of the momentum space for the cases 5 and 6. When $\bar{\omega}_p$ is instead increased for $\theta_0 < \theta_0^{\text{cr}}$, the \uparrow branch transforms via different ω -*diffusive* phases: Here, we get a mixing of the u_{\uparrow} (v_{\uparrow}) branch with the u_{\downarrow} (v_{\downarrow}) branch as in the panel 7, where there is a narrow region in \mathbf{k} space where the spectrum is diffusive and $\Re\omega \neq 0$. Note that for these spectral types the four branches cannot be degenerate all at the same time as in the *0-diffusive* case previously considered; now only two branches at the time get degenerate, while the other two do repel each other. Higher values of $\bar{\omega}_p$ induce a similar behaviour but for different intervals of momentum, as for region 8 or region 9. Degeneracy at zero energy is however still possible for the \downarrow branch, as seen in panels 8 and 9.

The spectral phases of a circularly (linearly) polarized fluid are the ones found on the line $\theta_0 = 0$ ($\theta_0 = \pi/4$) and coincide with the results discussed in Ref.¹⁸. After having classified completely all possible excitation spectra, we now discuss in the next section their intrinsic polarisation properties.

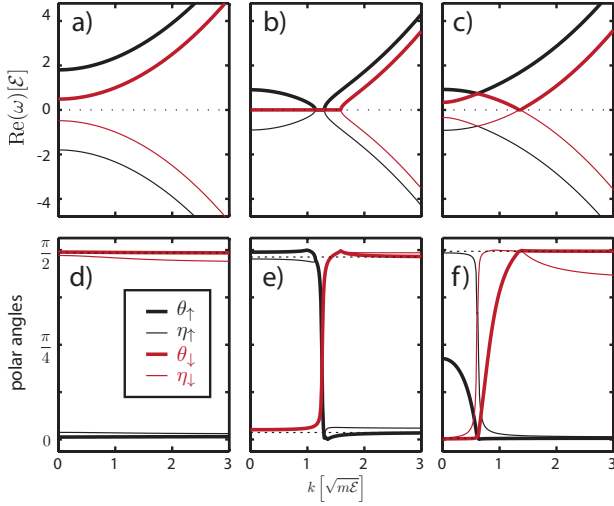


FIG. 5. (Color online) Bottom panels: Normal $\theta_{\uparrow,\mathbf{k}}$ (thick black lines) and $\theta_{\downarrow,\mathbf{k}}$ (thick red-gray) and antinormal $\eta_{\uparrow,\mathbf{k}}$ (thin black) and $\eta_{\downarrow,\mathbf{k}}$ (thin red-gray) polar angles for the *gapped* spectrum 1 (left panel), the *0-diffusive* spectrum 5 (middle panel), and the *ω -diffusive* spectrum 7 (right panel) of Fig. 4. For immediate comparison, each spectrum is replotted in the corresponding upper panels. The asymptotic large momentum behaviors for the normal angles (25) are plotted as black dashed line. The system parameters are $\alpha_2/\alpha_1 = -0.1$, $\mathbf{k}_p = 0$, $\gamma = 1.5$, and values of $(\bar{\omega}_p, \theta_0)$ as specified by the labels 1, 5 and 7 in the phase diagram of Fig. 3.

B. Degree of polarisation of collective excitations

Each mode of the collective spectrum does emit with an intrinsic degree of polarisation along the dispersion. This can be determined by starting from the eigenvalue equations,

$$\hat{\mathcal{L}}_{\mathbf{k}} \mathbf{x}_{\mathbf{k}}^{(a)} = \omega_{\mathbf{k}}^{(a)} \mathbf{x}_{\mathbf{k}}^{(a)}, \quad (22)$$

where $\omega_{\mathbf{k}}^{(a)}$ are the four branches (16) labeled by the index $a = u_{\uparrow}, v_{\uparrow}, u_{\downarrow}, v_{\downarrow}$ and $\mathbf{x}_{\mathbf{k}}^{(a)}$ are the four four-component eigenvectors of the Bogoliubov matrix $\hat{\mathcal{L}}_{\mathbf{k}}$, $\mathbf{x}_{\mathbf{k}}^{(a)} = (x_{u_{\pm},\mathbf{k}}^{(a)}, x_{v_{\pm},\mathbf{k}}^{(a)}, x_{u_{\mp},\mathbf{k}}^{(a)}, x_{v_{\mp},\mathbf{k}}^{(a)})$ — thus here the lower indices $u_{\pm}, v_{\pm}, u_{\mp}, v_{\mp}$ specify the eigenvector component, while the upper indices (a) refer to the eigenvalue branch.

For each branch labeled by (a) and for a given direction \mathbf{k} (measured with respect to the pump wave-vector \mathbf{k}_p) we might expect that, out of a 4-component complex vector $\mathbf{x}_{\mathbf{k}}^{(a)}$, the degree of polarisation will be characterised by two polar angles and by two azimuthal angles, all independent from each other. However, the particle-hole symmetry which characterises the Bogoliubov matrix (9) leads to a redundancy of parameters. In particular, the Bogoliubov matrix (9) is symmetric under the simultaneous exchange of the $u \leftrightarrow v$ components and the transformation $\hat{\mathcal{L}}_{\mathbf{k}} = -\hat{\mathcal{L}}_{\mathbf{k}}^*$. For eigenvalues and eigenvectors

this implies that

$$\begin{aligned} \omega_{-\mathbf{k}}^{(u_j)} &= -\omega_{\mathbf{k}}^{(v_j)*} \\ x_{u_{\pm},\mathbf{k}}^{(u_j)} &= -x_{v_{\pm},\mathbf{k}}^{(v_j)*}, \end{aligned}$$

where $j = \uparrow, \downarrow$. Thus, in order to characterise the intrinsic degree of polarisation of the collective spectrum, it is enough to define a “normal” polar polarisation angles for each of the two $j = \uparrow, \downarrow$ particle-like branches as

$$\cos(2\theta_{j,\mathbf{k}}) = |x_{u_{+},\mathbf{k}}^{(u_j)}|^2 - |x_{u_{-},\mathbf{k}}^{(u_j)}|^2. \quad (23)$$

In fact, for the hole-like branches, we have that $\cos(2\theta_{j,\mathbf{k}}) = |x_{v_{+},-\mathbf{k}}^{(v_j)}|^2 - |x_{v_{-},-\mathbf{k}}^{(v_j)}|^2$ — we are assuming here the following normalisation conditions for the eigenvector components, $|x_{u_{+},\mathbf{k}}^{(u_j)}|^2 + |x_{u_{-},\mathbf{k}}^{(u_j)}|^2 = 1 = |x_{v_{+},-\mathbf{k}}^{(v_j)}|^2 + |x_{v_{-},-\mathbf{k}}^{(v_j)}|^2$. Similarly, we can also define two “anti-normal” polar polarisation angles as:

$$I_{j,\mathbf{k}} \cos(2\eta_{j,\mathbf{k}}) = |x_{u_{+},\mathbf{k}}^{(v_j)}|^2 - |x_{u_{-},\mathbf{k}}^{(v_j)}|^2, \quad (24)$$

where $I_{j,\mathbf{k}} = |x_{u_{+},\mathbf{k}}^{(v_j)}|^2 + |x_{u_{-},\mathbf{k}}^{(v_j)}|^2 = |x_{v_{+},-\mathbf{k}}^{(u_j)}|^2 + |x_{v_{-},-\mathbf{k}}^{(u_j)}|^2$ is the normalisation of the anti-normal modes with respect to the normalisation of the normal ones which was fixed to 1. Thanks to the particle-hole symmetry, we could have equivalently defined these angles as $I_j \cos(2\eta_{j,\mathbf{k}}) = |x_{v_{+},-\mathbf{k}}^{(u_j)}|^2 - |x_{v_{-},-\mathbf{k}}^{(u_j)}|^2$. To summarise, for each branch we have two polar angles θ and η determining the degree of polarisation of the collective emission. These are not directly measurable quantities. However, in the pump-probe experiment proposed and analysed in the next section, the normal angle θ is related to the resonant transmission of the particle modes along the particle-like probe direction $\mathbf{k}_p + \mathbf{k}_{pb}$, while the anti-normal angle η to the transmission along the hole-like direction $\mathbf{k}_p - \mathbf{k}_{pb}$.

We now analyse in the bottom panels of Fig. 5, the behaviour of both $\theta_{j,\mathbf{k}}$ (thick lines) and $\eta_{j,\mathbf{k}}$ (thin lines) along each branch dispersion for three representative spectra (top panels) of the *gapped*, *0-diffusive*, and *ω -diffusive* types previously classified in Figs. 3 and 4. Let us first note that it can be easily shown that the intensity $I_{j,\mathbf{k}}$ decays quickly to zero at large momenta, i.e. $I_{j,\mathbf{k}} \sim k^{-4}$ for $k \gg \sqrt{m\mathcal{E}}$, where $\mathcal{E} = \alpha_1(|\psi_{+}|^2 + |\psi_{-}|^2)$. This implies that, in this limit, the coupling between particle-like and hole-like degrees of freedom can be neglected, allowing us to find the asymptotic behaviour of the normal polarisation angles at large momenta:

$$\begin{aligned} \lim_{k \gg \sqrt{m\mathcal{E}}} \cos(2\theta_{j,\mathbf{k}}) &= \frac{1 + \sigma_j \sqrt{1 + \xi^2}}{1 + \xi^2 + \sigma_j \sqrt{1 + \xi^2}} \\ \xi &= \frac{\alpha_2}{2\alpha_1 - \alpha_2} \tan(2\theta_0), \end{aligned} \quad (25)$$

where $\sigma_{j=\uparrow,\downarrow} = \pm 1$ and $\tan(2\theta_0) = 2|\psi_{+}||\psi_{-}|/(|\psi_{+}|^2 - |\psi_{-}|^2)$.

As panel (d) of Fig. 5 shows, for a *gapped* spectrum (panel (a)), corresponding to spectrum 1 in Fig. 4) the angles $\theta_{\uparrow,\mathbf{k}}$ (thick black line) and $\theta_{\downarrow,\mathbf{k}}$ (thick red-gray line) vary only very little along the dispersion because there is no mixing between \uparrow and \downarrow branches. In particular, while for the \uparrow branch the normal degree of polarisation (thick black) is almost everywhere fully left-polarised, $\theta_{\uparrow,\mathbf{k}} \simeq 0$ (corresponding to the north pole of the Poincaré sphere in Fig. 1), for the \downarrow branch (thick red-gray line) $\theta_{\downarrow,\mathbf{k}} \simeq \pi/2$ (south pole). Both anti-normal angles $\eta_{j,\mathbf{k}}$ (thin lines) also display a small variation along the dispersion from the values $\eta_{\uparrow,\mathbf{k}} \simeq 0$ (thin black) and $\eta_{\downarrow,\mathbf{k}} \simeq \pi/2$ (thin red-gray).

Mixing of the \uparrow and \downarrow branches causes instead sudden changes of both normal and antinormal angles along each dispersion. This is the case of both the 0-*diffusive* spectrum shown in panel (b) of Fig. 5 (corresponding to panel 5 of Fig. 4) as well as the ω -*diffusive* spectrum shown in panel (c) (and corresponding to the spectrum 7 of Fig. 4), even if the mixing happens in different ways. In particular, for the 0-*diffusive* spectrum, different branches touch each other in two separated regions in \mathbf{k} -space. The branches u_{\downarrow} and v_{\downarrow} mix together for $k \lesssim 1.5\sqrt{m\mathcal{E}}$, where the angles $\theta_{\downarrow,\mathbf{k}}$ and $\eta_{\downarrow,\mathbf{k}}$ coincide. Inside this region, there is another region where also the u_{\uparrow} and v_{\uparrow} mix together. Here, also the angles $\theta_{\uparrow,\mathbf{k}}$ and $\eta_{\uparrow,\mathbf{k}}$ will coincide. In between these mixing regions, the values of the angles undergo a sudden change in value from almost a purely left-circularly polarised degree to a right-circularly polarised degree.

The last case we analyse is the ω -*diffusive* spectrum shown in panel (c) of Fig. 5. The difference with the case previously considered of a 0-*diffusive* spectrum, lies in the fact that now all four real part branches do not become degenerate in the same momentum region and that the degeneracy of \uparrow and \downarrow branches is allowed at finite energy. Aside these differences in how \uparrow and \downarrow branches do mix with each other, we observe in panel (f) a similar sudden flip of both normal and anti-normal polar angles along the dispersion that we also observed for the 0-*diffusive* spectrum in panel (e).

C. Probe response

After having discussed the intrinsic properties of the collective spectrum, including the emission degree of polarisation along the dispersion of each branch, we derive now the response of the spinor fluid to an additional probe beam and how this is related to the intrinsic spectral properties discussed so far. To this end, we go back to the system linear response (8) to a weak external probe shined at a direction $\mathbf{k}_p + \mathbf{k}_{pb}$ and an energy $\omega_p + \omega_{pb}$. Eq. (8) can be easily inverted to give the system response $\mathbf{w} = (u_+, v_+, u_-, v_-)^T$ in terms of the probe vector $\mathbf{f}^{pb} = (f_+^{pb}, 0, f_-^{pb}, 0)^T$:

$$\mathbf{w} = \left(\omega_{pb} \hat{\mathbb{I}} - \hat{\mathcal{L}}_{\mathbf{k}_{pb}} \right)^{-1} \mathbf{f}^{pb}. \quad (26)$$

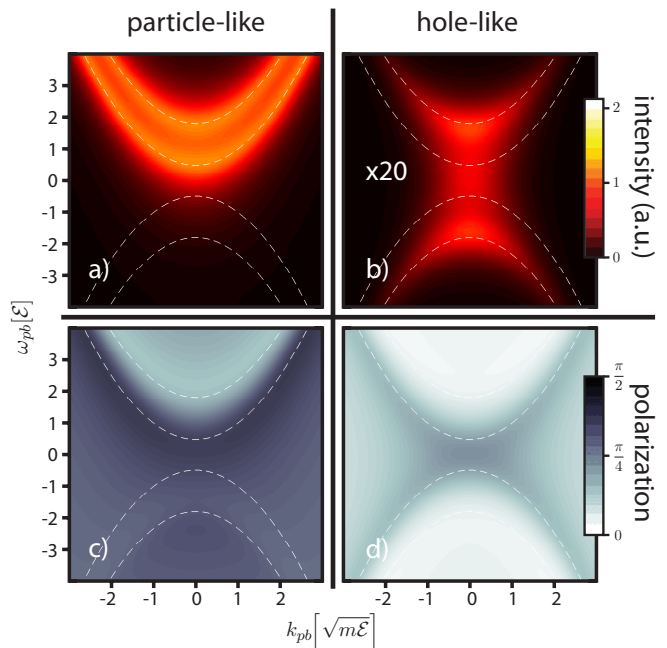


FIG. 6. (Color online) Response to a probe beam for a *gapped* spectrum of excitations. Two-dimensional maps of the particle-like I_u (panel (a)) and hole-like I_u (panel (b)) intensities, and of the polar angles along the \mathbf{k}_{pb} direction θ_u (panel (c)) and the $-\mathbf{k}_{pb}$ direction θ_v (panel (d)) as a function of both the probe momentum \mathbf{k}_{pb} and energy ω_{pb} . The system parameters are the same ones fixed in panels (a) and (d) of Fig. 5, the probe is linearly polarized ($\theta_{pb} = \pi/4$) and the polariton decay rate is set to $\gamma = 1.5\mathcal{E}$. White dashed lines are the real part of the excitation spectrum $\Re\omega_{\mathbf{k}}^{(a)}$. Note that the intensity of the hole-like signal has been multiplied by a factor 20 with respect to the particle-like to obtain a clearer contrast.

As explained previously, and also illustrated in the schematic set-up of Fig. 2, the intensity of the response in the direction $\mathbf{k}_p + \mathbf{k}_{pb}$ will be given by the particle-like component $|u_{\pm}|^2$, while the one at the direction $\mathbf{k}_p - \mathbf{k}_{pb}$, by the hole-like component $|v_{\pm}|^2$ — from now onwards, we will consider the particular case of a pump shined orthogonally to the cavity plane, $\mathbf{k}_p = 0$. From Eq. (26), we expect that the response will be enhanced when $(\omega_{pb}, \mathbf{k}_{pb})$ is scanned close to one of the branches of the collective excitation spectrum, i.e., the eigenvalues of the Bogoliubov matrix $\hat{\mathcal{L}}_{\mathbf{k}_{pb}}$. Because the spectrum is complex, we expect a broadened enhanced emission — typically of the order of the polariton linewidth γ , with variations in the diffusive regions in momentum space where different branches touch each other and the imaginary part of the spectrum deviates from the polariton lifetime γ . While the resolution in energy is limited by the imaginary part of the spectrum, the resolution in momentum space can only suffer experimental limitations, such as the angular resolution of the detection device and the intrinsic angular width of the probe beam. The probe beam resolution in momentum can be improved by considering a large

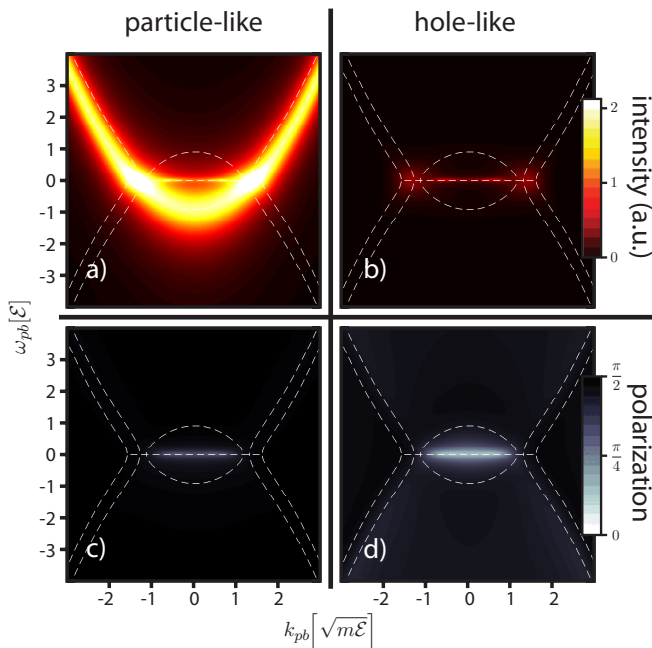


FIG. 7. Response to a probe beam for a 0-*diffusive* spectrum of excitations. Two-dimensional maps of the particle-like I_u (panel (a)) and hole-like I_v (panel (b)) intensities, and of the polar angles along the \mathbf{k}_{pb} direction θ_u (panel (c)) and the $-\mathbf{k}_{pb}$ direction θ_v (panel (d)) as a function of both the probe momentum \mathbf{k}_{pb} and energy ω_{pb} . The system parameters are the same ones fixed in panels (b) and (e) of Fig. 5, the probe purely circularly right-polarized ($\theta_{pb} = \pi/2$) and the polariton decay rate is set to $\gamma = 1.5\mathcal{E}$. White dashed lines are the real part of the excitation spectrum $\Re\omega_{\mathbf{k}}^{(a)}$.

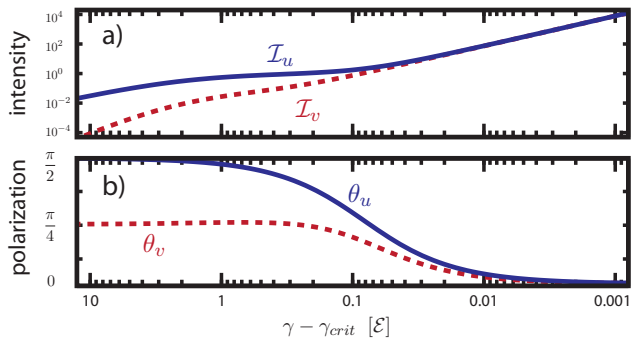


FIG. 8. Intensities $I_{u,v}$ (panel (a)) and polar angles $\theta_{u,v}$ (panel (b)) for the 0-*diffusive* spectrum of excitations shown in Fig. 7 at fixed values of the probe momentum $\mathbf{k}_{pb} = 0.5\sqrt{m}\mathcal{E}$ and energy $\omega_{pb} = 0$ as a function of the rescaled polariton decay rate $\gamma - \gamma_{crit}$, where $\gamma_{crit} \simeq 1.39\mathcal{E}$.

enough homogeneous profile²⁹.

We express the probe vector \mathbf{f}^{pb} in terms of the polar θ_{pb} and azimuthal ϕ_{pb} angles, quantifying the polarisation degree of the probe:

$$\mathbf{f}^{pb} = |f^{pb}|(\cos 2\theta_{pb}, 0, e^{i\phi_{pb}} \sin 2\theta_{pb}, 0)^T, \quad (27)$$

where $|f^{pb}|^2$ is the probe beam intensity. We set $\phi_{pb} = 0$. Similarly, the response \mathbf{w} can be conveniently parametrised in terms of the particle-like $I_u = |u_+|^2 + |u_-|^2$ and hole-like $I_v = |v_+|^2 + |v_-|^2$ intensities, as well as the polar angles $\theta_{u,v}$ along the two directions $\pm\mathbf{k}_{pb}$:

$$I_u \cos(2\theta_u) = |u_+|^2 - |u_-|^2 \quad (28)$$

$$I_v \cos(2\theta_v) = |v_+|^2 - |v_-|^2. \quad (29)$$

Finally, as already discussed, we assume that the pump induces a mean-field state with $\phi_0 = 0$ and $\theta_0 \in [0, \pi/4]$ (4).

We plot in Figs. 6 and 7 the two-dimensional maps for both intensities $I_{u,v}$ and polar angles $\theta_{u,v}$ for the response to a probe beam by scanning different values of the probe energy ω_{pb} and momentum \mathbf{k}_{pb} . We choose the particular case of a *gapped* spectrum (Fig. 6), corresponding to the same conditions as panels (a) and (d) of Fig. 5 and the case of a 0-*diffusive* spectrum (Fig. 7), corresponding to the same conditions as panels (b) and (e) of Fig. 5. We first note that, as expected, the probe beam (27) has only a finite strength in the particle-like channels and cannot directly excite hole-like quasi-particles. Nevertheless, the response has a finite emission intensity also for the hole-like branches because of the interactions mixing together particle and hole degrees of freedom. As previously illustrated in Eq. (19) particle and hole modes asymptotically decouple one from the other at large momenta. We thus expect that the response emission intensity quickly drops to zero for all hole-like branches. In panel (b) of Fig. 6 this behaviour is clearly visible, as the emission intensity of the hole branches is strongly reduced with respect to the one of the particle branches.

In the previous section we have seen that each branch of the collective excitation spectrum is characterised by an intrinsic degrees of polarization, quantified by the normal ($\theta_{\uparrow,\downarrow}$) and anti-normal ($\eta_{\uparrow,\downarrow}$) polar angles. In Fig. 6, the *gapped* spectrum is probed with a linearly polarized beam, $\theta_{pb} = \pi/4$. Here, we obtained an enhanced emission when the probe is in resonance with either the u_{\uparrow} or the u_{\downarrow} branch. We remind that for a *gapped* spectrum there is no mixing between the \uparrow and \downarrow degrees of freedom, and thus the $\theta_{\uparrow,\downarrow}$ angles only weakly deviate from their asymptotic values at large \mathbf{k} (see Fig. 5), in this particular case almost purely circularly left or right polarized. Hence, one expects that the emission intensity for the u_{\uparrow} and u_{\downarrow} branches is comparable, since the linearly polarised probe couples identically to left- and right-polarized modes. In panel (c) of Fig. 6 we observe the polarization to undergo a rotation when in resonance with one of the spectral branches. As expected, probing at resonance with the u_{\uparrow} branch results in a largely left-polarized emission, while the u_{\downarrow} branch induces a right-circular polarization.

Interesting effects are observed for the case of diffusive spectra, and we show in particular the case of a 0-*diffusive* spectrum in Fig. 7. For this case we consider the case of

a right-circularly polarized probe beam ($\theta_{pb} = \pi/2$) so that we have a u_\downarrow branch emitting much stronger than the u_\uparrow branch (see panel (a) of Fig. 7). However, around $\mathbf{k}_p = 0$, where the spectral branches mixed one the other in a diffusive region, we see that the resonant branch is not u_\downarrow , rather v_\uparrow . Here, the strongest emission intensity comes from the u_\downarrow branch at large momenta and from the v_\uparrow branch inside the diffusive region at small \mathbf{k} . Because of the mixing between \uparrow and \downarrow degrees of freedom, we have observed a sudden spin flip for the degree of polarisation of the eigenvectors around $|\mathbf{k}| \sim 1.2\sqrt{m\mathcal{E}}$. This is the reason for the resonant emission transfers from u_\downarrow to v_\uparrow at small \mathbf{k} . From panel (b) of Fig. 7 it is clear that, in the beam transferred in the $-\mathbf{k}_{pb}$ direction, the emission is the strongest in the diffusive momentum ring at $\omega_p = 0$ where u_\downarrow and v_\downarrow are mixed. The stronger intensity for these modes can be explained in terms of an onset of parametric amplification. In fact, in this diffusive region the imaginary part of the spectrum part deviates from the value of the constant decay rate and there is an additional contribution from the negative argument of the outer root in Eq. (16) — see panel 5 in Fig. 4. For this reason, these modes acquire a longer lifetime, and therefore undergo enhanced scattering. Similarly, in panel (a) of Fig. 7, one can appreciate an increase in transmission in the same diffusive region. In addition, there is also an increased emission on the diffusive region at $\omega_p = 0$ where the u_\downarrow and v_\downarrow branches are degenerate. Although, for these values of the momentum, these branches are circularly left polarized, the inter-spin interaction coupling the \uparrow and \downarrow modes, combined with the strong parametric amplification, still leads to a strong emission. It is interesting to note that in previous work¹², the proximity to an instability to a parametric scattering regime has been related to the occurrence of a negative drag force when a resonantly pumped polariton fluid scatters against a localised defect. Here, the same phenomenon leads to enhanced emission of parametrically amplified modes when the system is probed with an additional weak laser.

In panels (c) [(d)] of Fig 7 we plot the azimuthal polarization angle for particle-like (hole-like) transmitted signal at \mathbf{k}_{pb} ($-\mathbf{k}_{pb}$). The resonant branch is u_\downarrow at large \mathbf{k} and v_\uparrow for small values of the momentum and strongly emits circularly right polarized light — $\theta_{pb}^u \simeq \theta_{pb}^v \simeq \pi/2$. Yet the parametrically amplified region around $\mathbf{k}_p = 0$ emits both in the transmitted \mathbf{k}_{pb} and $-\mathbf{k}_{pb}$ directions an almost purely circularly left polarized light. Hence, the parametric amplification of the mixed u_\downarrow and v_\downarrow mode causes the left-polarized incoming probe light to undergo a spin flip when interacting with the polariton sample. We show in Fig. 8 that $\theta_{pb}^{u,v}$ tend to 0 (i.e., almost pure left-polarization), when the parametric amplified mode $\mathbf{k}_p = 0.5\sqrt{m\mathcal{E}}$, probed with $\omega_{pb} = 0$, is brought closer to resonance by varying the polariton decay time $\gamma \rightarrow \gamma_{crit}^-$ — here γ_{crit} is the minimum value of the polariton decay rate required for the system stability, i.e., $\Im\omega < 0$. The emission intensity (panel (a) of Fig. 8) diverges as $1/(\gamma - \gamma_{crit})^2$ for both particle-like and hole-like signals

when they are brought close to resonance. This can be understood from the expression (26), where we see that the right-hand side becomes singular if ω_{pb} equals $\Re\omega_{\mathbf{k}_{pb}}^{(a)}$ and at the same time $\Im\omega_{\mathbf{k}_{pb}}^{(a)} \rightarrow 0^-$. In this limit, the response \mathbf{w} coincides with the eigenvector $\mathbf{x}^{(a)}$ of the Bogoliubov matrix $\hat{\mathcal{L}}_{\mathbf{k}_{pb}}$. Here, this is the case for \mathbf{x}^{u-} , so that the polarization θ_{pb} of the response approaches $\theta_{\downarrow|\mathbf{k}=0} = \eta_{\downarrow|\mathbf{k}=0} \simeq 0.08$, as it can be seen in panel (b) of Fig. 8. Note that $\theta_{\downarrow} = \eta_{\downarrow}$ exactly in the diffusive disk around $\mathbf{k} = 0$, where u_\downarrow and v_\downarrow coincide. In Fig. 8, we have measured the decay rate γ in units of self-interaction energy \mathcal{E} .

Experimentally, however, γ is fixed for a given microcavity, but the ratio γ/\mathcal{E} can be tuned by varying the laser pump power, $|f^p|^2$ in Eq. (2). One should then calculate the mean-field equations (3) to derive the polariton spin densities $|\psi_\pm|^2$ and thus the self-interaction energy \mathcal{E} . By varying the tilting angle of the probe beam with respect to the pump, one can scan through \mathbf{k} -space. As depicted on Fig. 2, also the detectors should be placed accordingly: one at the same angle as the probe and the other at the mirrored angle, to detect the particle and the hole-like signal respectively. At each position of the probe, a vertical slice on the response figures can be reconstructed by changing the probe frequency ω_{pb} and measuring the intensity and polarization at both detectors.

IV. CONCLUSIONS

We have analytically derived the spectrum of elementary excitations for a spinor polariton fluid in the linear response approximation scheme. For fixed interaction strength, the spectra can be classified in terms of two dimensionless parameters only: mean-field polarization angle and the renormalised pump detuning. Even though there is a large variety of possible spectra, we identify three major classes, *gapped*, *0-diffusive*, and *ω -diffusive*, depending how the opposite polarisation spectral branches mix together and at which energy. For *0-diffusive* the mixing happens at zero energies, for *ω -diffusive* it happens at finite energy. Interestingly, only the mean-field polarization is sufficient to distinguish between these two different diffusive-like spectra. We show that the mixing of \uparrow and \downarrow branches characterises sudden spin flips of the intrinsic degree of polarisation along the branches for both diffusive-like spectra. We have characterised the response of the system to an external probe in terms of the spectral intrinsic properties. In particular, we have shown that the intrinsic polarization of an elementary excitation is reflected in the transmitted signal of a probe beam experiment. For *gapped* spectra the degree of polarisation varies only very weakly along each branches. In contrast, for both *0-diffusive* and *ω -diffusive* spectra, the strong mixing between opposite polarisation branches at small momenta leads to a spin flip of the

transmitted degree of polarisation along the branch. The closer the polariton spinor fluid is to a parametric instability, the larger the amount of spin flip is, independently of the degree of polarisation of the probing beam.

Recently numerous fascinating results have been achieved in the study of the response of a spinor polariton fluid to a magnetic field, such as the spin Meissner effect²⁴ and effective magnetic monopoles²³. As a future perspective, it could be interesting to include the Zeeman-splitting terms in our model and study their influence on the spectrum of excitations. In addition, also effects of disorder^{30,31} and TE-TM splitting could be in-

corporated.

ACKNOWLEDGMENTS

MVR gratefully acknowledges support in the form of a Ph. D. fellowship of the Research Foundation - Flanders (FWO). MW acknowledges financial support from the FWO-Odysseus program. F.M.M. acknowledges financial support from the Ministerio de Economía y Competitividad (MINECO) (Contract No. MAT2011-22997) and the Comunidad Autónoma de Madrid (CAM) (Contract No. S-2009/ESP-1503).

-
- * Mathias.VanRegemortel@uantwerpen.be
- ¹ A. V. Kavokin, J. J. Baumberg, G. Malpuech, and F. P. Laussy, *Microcavities* (Oxford University Press, Oxford, 2007).
 - ² J. Keeling, F. M. Marchetti, M. H. Szymańska, and P. B. Littlewood, *Semicond. Sci. Technol.* **22**, R1 (2006).
 - ³ J. Keeling and N. G. Berloff, *Contemporary Physics* **52**, 131 (2011), <http://dx.doi.org/10.1080/00107514.2010.550120>.
 - ⁴ I. Carusotto and C. Ciuti, *Rev. Mod. Phys.* **85**, 299 (2013).
 - ⁵ I. Carusotto and C. Ciuti, *Phys. Rev. Lett.* **93**, 166401 (2004).
 - ⁶ C. Ciuti and I. Carusotto, *physica status solidi (b)* **242**, 2224 (2005).
 - ⁷ A. Amo, J. Lefrère, S. Pigeon, C. Adrados, C. Ciuti, I. Carusotto, R. Houdré, E. Giacobino, and A. Bramati, *Nat. Phys.* **5**, 805 (2009).
 - ⁸ S. Pigeon, I. Carusotto, and C. Ciuti, *Phys. Rev. B* **83**, 144513 (2011).
 - ⁹ A. Amo, S. Pigeon, D. Sanvitto, V. G. Sala, R. Hivet, I. Carusotto, F. Pisanello, G. Leménager, R. Houdré, E. Giacobino, C. Ciuti, and A. Bramati, *Science* **332**, 1167 (2011).
 - ¹⁰ G. Nardin, G. Grosso, Y. Leger, B. Pietka, F. Morier-Genoud, and B. Deveaud-Plédran, *Nature Physics* **7**, 635 (2011).
 - ¹¹ D. Sanvitto, S. Pigeon, A. Amo, D. Ballarini, M. D. Giorgi, I. Carusotto, R. Hivet, F. Pisanello, V. G. Sala, P. S. Soares-Guimaraes, R. Houdre, E. Giacobino, C. Ciuti, A. Bramati, and G. Gigli, *Nature Photonics* **5**, 610 (2011).
 - ¹² M. Van Regemortel and M. Wouters, *Phys. Rev. B* **89**, 085303 (2014).
 - ¹³ N. Gippius, I. Shelykh, D. Solnyshkov, S. Gavrillov, Y. Rubo, A. Kavokin, S. Tikhodeev, and G. Malpuech, *Phys. Rev. Lett.* **98**, 236401 (2007).
 - ¹⁴ D. Sarkar, S. S. Gavrillov, M. Sich, J. H. Quilter, R. A. Bradley, N. A. Gippius, K. Guda, V. D. Kulakovskii, M. S. Skolnick, and D. N. Krizhanovskii, *Phys. Rev. Lett.* **105**, 216402 (2010).
 - ¹⁵ A. Amo, T. C. H. Liew, C. Adrados, R. Houdr, E. Giacobino, A. V. Kavokin, and A. Bramati, *Nature Photonics* **4**, 361 (2010).
 - ¹⁶ T. Ostatnický, I. Shelykh, and A. Kavokin, *Phys. Rev. B* **81**, 125319 (2010).
 - ¹⁷ N. Takemura, S. Trebaol, M. Wouters, M. T. Portella-Oberli, and B. Deveaud, *Nat Phys* **10**, 500 (2014).
 - ¹⁸ D. Solnyshkov, I. Shelykh, N. Gippius, A. Kavokin, and G. Malpuech, *Phys. Rev. B* **77**, 045314 (2008).
 - ¹⁹ I. A. Shelykh, A. V. Kavokin, Y. Rubo, T. C. H. Liew, and G. Malpuech, *Semicond. Sci. Technol.* **25**, 013001 (2010).
 - ²⁰ C. Ciuti, V. Savona, C. Piermarocchi, A. Quattropani, and P. Schwendimann, *Phys. Rev. B* **58**, 7926 (1998).
 - ²¹ M. Vladimirova, S. Cronenberger, D. Scalbert, K. V. Kavokin, A. Miard, A. Lemaître, J. Bloch, D. Solnyshkov, G. Malpuech, and A. V. Kavokin, *Phys. Rev. B* **82**, 075301 (2010).
 - ²² C. Pethick and H. Smith, *Bose-Einstein condensation in dilute gases* (Cambridge University Press, 2002).
 - ²³ D. Solnyshkov, H. Flayac, and G. Malpuech, *Phys. Rev. B* **85**, 073105 (2012).
 - ²⁴ J. Fischer, S. Brodbeck, A. V. Chernenko, I. Lederer, A. Rahimi-Iman, M. Amthor, V. D. Kulakovskii, L. Worschech, M. Kamp, M. Durnev, C. Schneider, A. V. Kavokin, and S. Höfling, *Phys. Rev. Lett.* **112**, 093902 (2014).
 - ²⁵ T. K. Paraïso, M. Wouters, Y. Léger, F. Morier-Genoud, and B. Deveaud-Plédran, *Nat Mater* **9**, 655 (2010).
 - ²⁶ M. Wouters and I. Carusotto, *Phys. Rev. A* **76**, 043807 (2007).
 - ²⁷ A. C. Berceanu, E. Cancellieri, and F. M. Marchetti, *Journal of Physics: Condensed Matter* **24**, 235802 (2012).
 - ²⁸ L. D. Landau and E. M. Lifshitz, *Fluid Mechanics, Second Edition: Volume 6 (Course of Theoretical Physics)*, 2nd ed., Course of theoretical physics / by L. D. Landau and E. M. Lifshitz, Vol. 6 (Butterworth-Heinemann, 1987).
 - ²⁹ M. Wouters and I. Carusotto, *Phys. Rev. B* **75**, 075332 (2007).
 - ³⁰ D. Solnyshkov, I. Shelykh, and G. Malpuech, *Phys. Rev. B* **80**, 165329 (2009).
 - ³¹ Y. G. Rubo, A. Kavokin, and I. Shelykh, *Physics Letters A* **358**, 227 (2006).